Vol. 3 • No. 12 • June 21 • 2016

www.advmatinterfaces.de

# ADVANCED MATERIALS INTERFACES

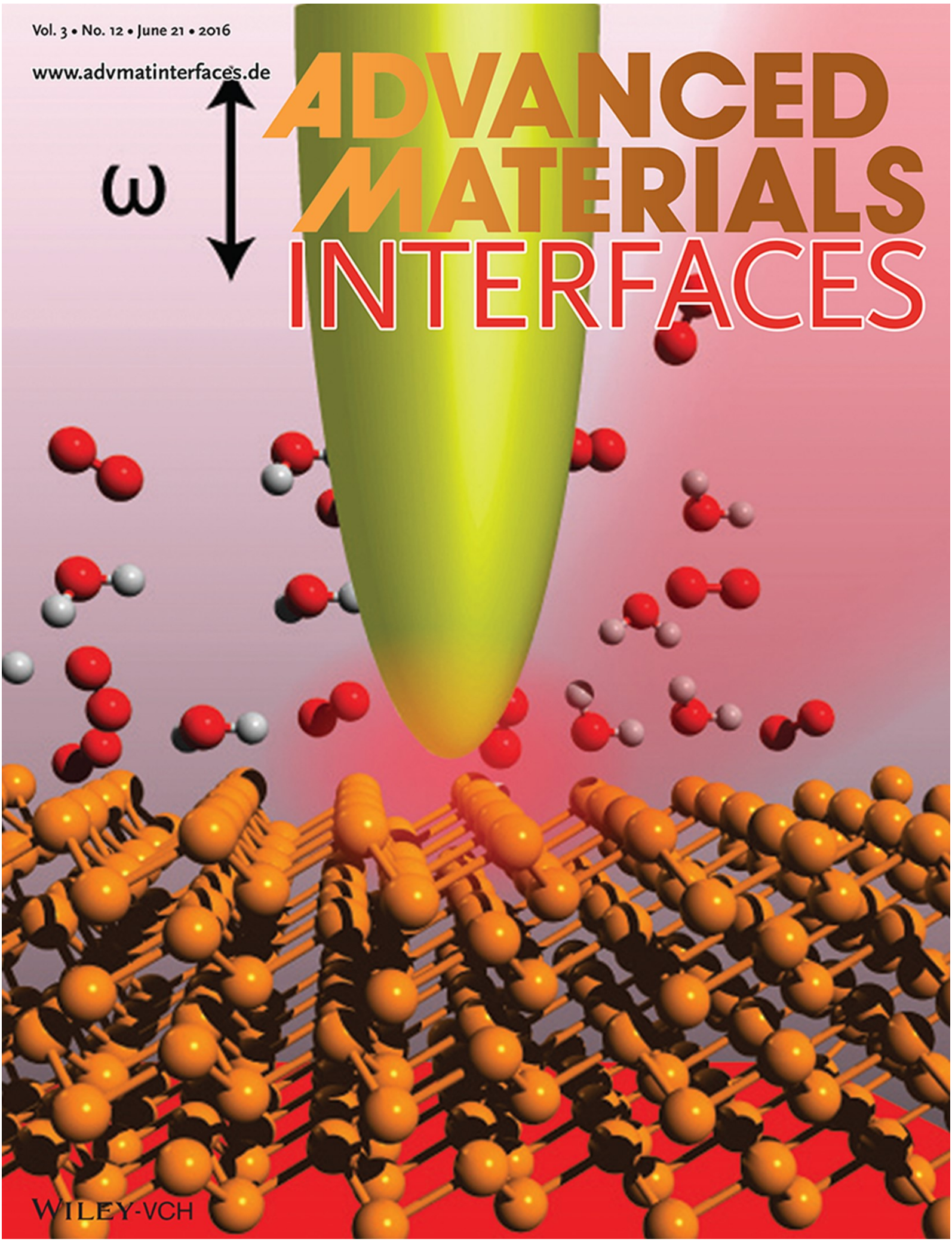


WILEY-VCH

# Nanoscopy of Black Phosphorus Degradation

*Sampath Gamage, Zhen Li, Vladislav S. Yakovlev, Colin Lewis, Han Wang, Stephen B. Cronin, and Yohannes Abate**

Among numerous van der Waals materials that have been identified lately, black phosphorus (BP) has generated intense interest for various optoelectronic applications due to its outstanding physical properties. Its tunable, direct, and narrow band gap makes it an attractive semiconductor for nanoelectronics and nanophotonics applications.[1–3] Similar to other 2D layered materials, BP can be prepared by simple mechanical exfoliation with additional exotic features such as its extraordinary in-plane anisotropic electrical, optical, and vibrational properties.[4–7] The major impediment to research and prospective application of single/few-layer BP is its chemical degradation under ambient conditions.[8] An extensive understanding of the degradation process and reliable ways to achieve stable and scalable degradation protection is necessary in order to realize the full potential of this material in its single- and few-layer forms. Recent studies have shed light on the underlying mechanism and speed of degradation by atomic force microscopy (AFM) and spectroscopic techniques.[8,9] Few passivation methods have also been investigated with various degree of success to slow down and prevent degradation.[3] Breakthroughs in developing powerful passivation methods to overcome this degradation issue require deeper experimental understanding and theoretical modeling of the degradation process as well as the effectiveness of passivation techniques.

We report the first experimental quantification of geometric properties and theoretical modeling of the chemical degradation process of BP and investigate the effectiveness of passivation coatings using infrared scattering type scanning near-field microscopy (s-SNOM).[10,11] We chemically identify oxidized phosphorus species locally at the onset of degradation by nanoscale spectroscopic imaging at mid-infrared frequencies. We found that these species can form underneath 5 nm thick $Al_2O_3$ coating deposited by atomic layer deposition (ALD) indicating that thin coating is insufficient to protect BP against degradation caused by ambient medium. By performing simultaneous topographic and optical time series imaging over several months, we show that a nanolayer BP exposed to ambient environment degrades at a steadily increasing rate until saturation begins, so that the degraded area and volume of degraded regions as functions of time follow the well-known S-shaped growth curve (sigmoid growth curve).[12] Phenomenological modeling of experimental results suggests a strong influence of degraded areas on adjacent BP. Our model is advantageous since it is based on elementary probabilities that can be related to the $O_2$ and $H_2O$ content in the ambient medium, as well as to the chemical reaction processes that result in oxidized phosphorus species. Therefore, our phenomenological model can, in principle, be used to predict the degradation time under different environmental conditions. Our work incorporates experimentally measured geometric patterns of BP degradation with model prediction allowing us to determine the growth saturation value, steepness of the growth, and the mid-point of the growth, and the relative importance of neighboring interactions.

Mechanical exfoliation was used for BP sample preparation on an Si substrate. After the exfoliation, the substrates were loaded in to ALD chamber (Cambridge NanoTech, Savannah 200) immediately for the $Al_2O_3$ deposition with TMA (trimethyl aluminum) and water as precursors. For the first three rounds, only TMA is flowed through the chamber to prevent oxidization of the BP flakes. The ALD was performed at 200 °C. Various thicknesses (1, 5, 10, 20, 50, and 100 nm) of $Al_2O_3$ were coated on the BP flakes using ALD. Topographic and near-field optical images were acquired using a commercial s-SNOM system (neaspec.com). An AFM tip coated with PtIr, oscillating at resonance frequency of $f \approx 280$ kHz, is irradiated by a focused quantum cascade laser (QCL) laser at 45° with respect to the sample surface (**Figure 1**a). The scattered signal from the tip–sample interface region is demodulated at high harmonics of the tip resonance frequency (*nf, n > 1*) and detected by phase-modulation (pseudo-heterodyne) interferometry, producing simultaneous topography, optical amplitude, and phase images.

We performed infrared (IR) optical amplitude and phase resolved near-field spectroscopy imaging of unencapsulated BP flake left to degrade in order to chemically identify the degraded region in BP in the laser wavelength range, $\lambda = 5.5 - 10.8$ μm. Figure 1b shows a topography image and Figure 1c simultaneously recorded IR third harmonic amplitude and phase optical images of a 10 nm thick BP flake left to degrade for some time in ambient environment. Although the various AFM height distributions shown in the topography and line profile images in Figure 1b are not sufficient to identify the chemical composition of nano-islands, taller topographic protrusions on BP samples exposed to ambient environment have been used to

S. Gamage, C. Lewis, Prof. Y. Abate
Department of Physics and Astronomy
Center for Nano Optics
Georgia State University
Atlanta, GA 30303, USA
E-mail: yabate@gsu.edu
Z. Li, Prof. H. Wang, Prof. S. B. Cronin
Viterbi School of Engineering
University of Southern California
Los Angeles, CA 90089, USA
Dr. V. S. Yakovlev
Center for Nano-Optics
Georgia State University
Atlanta, GA 30303, USA

**DOI: 10.1002/admi.201600121**

  

ADVANCED MATERIALS INTERFACES
www.advmatinterfaces.de

Materials Views
www.MaterialsViews.com

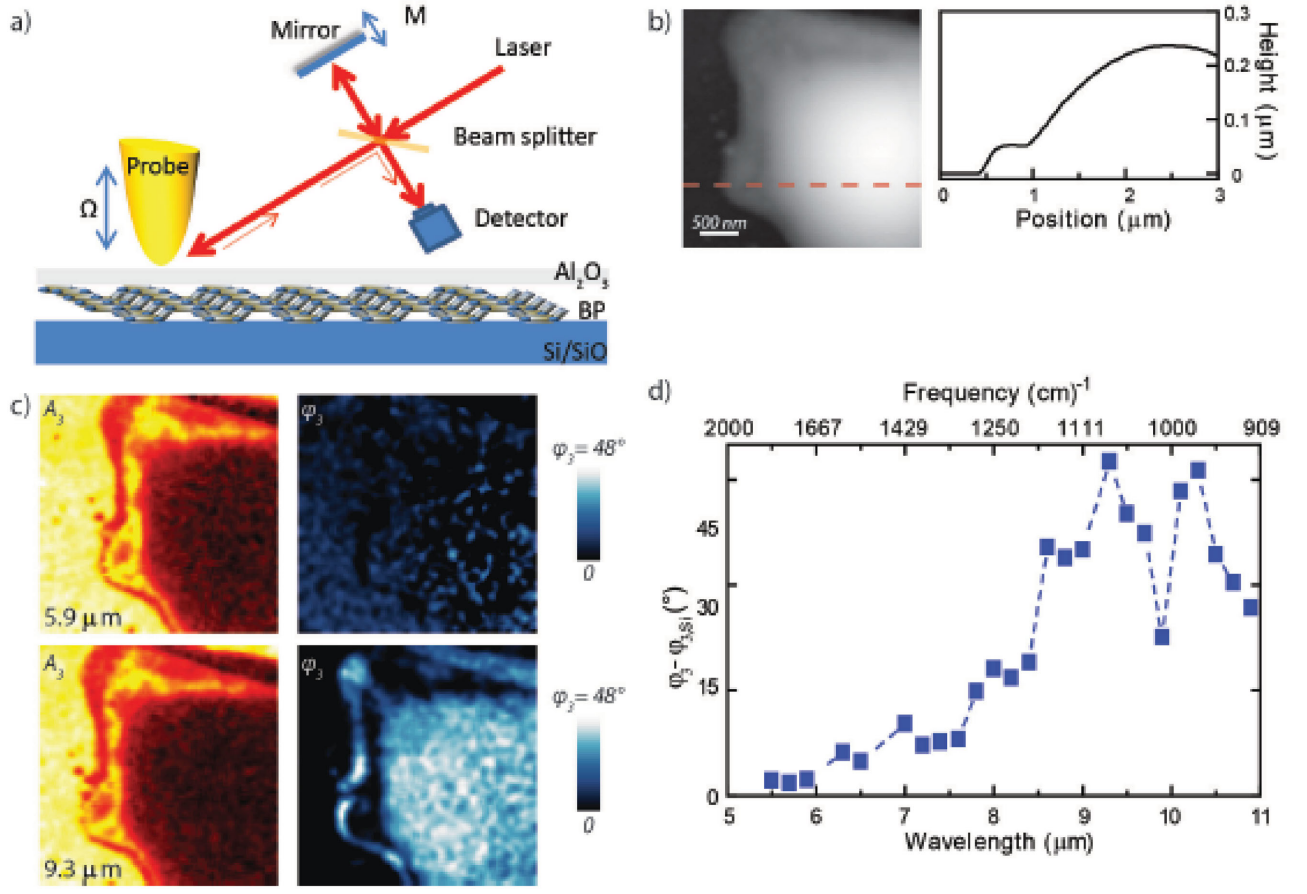


**Figure 1.** a) Schematic of the s-SNOM experimental setup vertically polarized laser focused on the tip–sample junction produces a near-field interaction with the sample surface, allowing mapping of the local dielectric values of BP surface. b) Topography image and line profile plot. c) Third harmonic optical amplitude ($A_3$) and phase ($\phi_3$) images at illumination laser wavelength 5.9 and 9.3 μm. d) Normalized s-SNOM phase ($\phi_3$) spectroscopy plot of degraded BP.

identify degraded regions.[8] The unique capability of s-SNOM is its ability to allow spectroscopic identification of islands at nanometer resolution regardless of the excitation wavelength used.[10,13] Figure 1c shows third harmonic optical near-field amplitude and phase images recorded simultaneously with topography at two laser wavelengths, 5.9 and 9.3 μm. In both amplitude images, topographically higher BP nano-islands appear darker than the substrate. Such a negative contrast in the amplitude images is due to smaller dielectric constant of the darker island compared to the bright region as it is well known in s-SNOM imaging. The near-field amplitude contrast coupled with the observed topographic protrusions, indicate that taller islands have different material makeup due to ambient exposure. Further chemical identification is provided by the near-field phase images, which show a clear optical contrast difference between the images taken at the two wavelengths in Figure 1c. In the phase image taken at 9.3 μm we observe a clear contrast between the islands, which nearly vanishes at 5.9 μm. In s-SNOM the phase spectral contrast indicates an absorption in the sample that could be caused by a vibrational mode. To map the absorption spectral response of the sample, we performed phase spectroscopic imaging in the laser wavelength range, $\lambda$ = 5.5–10.8 μm. Figure 1d shows the experimental near-field optical phase spectrum taken at the degraded parts of the sample normalized by the background phase on the Si substrate. We find a broad near-field phase resonant spectrum that starts around ≈7.5 μm. The near-field phase resonance is similar to the far-field absorption peak. This broad infrared band is best assigned to phosphate species that resulted due to ambient degradation following the assignment made in ref. [8]. Using high-resolution s-SNOM, we investigated the time evolution of degradation of an unencapsulated exfoliated 27 nm thick BP flake in an ambient environment over the course of several months (>3 months). **Figure 2** displays the topography (Figure 2a–k) and near-field optical images (Figure 2l–v) taken at a laser wavelength of $\lambda$ = 10.5 μm imaged over a time span of 90 d since exfoliation. In the topographic images, the degraded regions are easily distinguishable from the undegraded regions by higher topography (Figure 2a–j) and lower (darker) contrast in the near-field images (Figure 2k–t). The degradation begins soon after exfoliation as nano-sized particles that appear randomly on the surface (Figure 2a). The density of these degraded BP nanoparticles (number of degraded BP nanoparticles/unit area) is high in the first few days (1–5 d), however at the intermediate stage (≈5–15 d) the nanoparticles density decreases as some of the particles start to become rapidly larger by coalescing with the

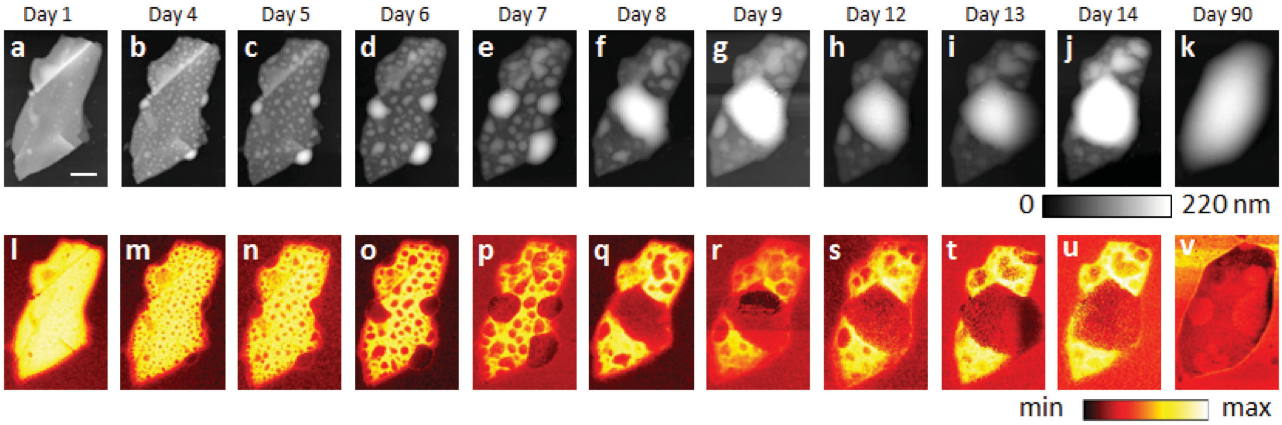


**Figure 2.** a–k) Time evolution of topography and l–v) near-field third harmonic optical amplitude taken at laser wavelength of $\lambda = 10.5$ μm of freshly exfoliated unencapsulated BP with thickness ≈27 nm. Scale bar = 500 nm.

neighboring degraded regions and eventually degradation covering all of the surface (Figure 2k,v). We plotted the measured fraction of the degraded area as a function of time in **Figure 3**. Each data point on the plot (dark squares) represents the sum of the measured area of each degraded bubble divided by the total area of the sample. The degraded surface area was measured using the change in the height of a given location on the sample by setting a threshold value for height as a threshold for each scan. The experimental graph shows that the degraded area percentage increases with time slowly in the beginning and much faster afterward before saturating. Similar degradation behavior was observed in other flakes with comparable thicknesses.

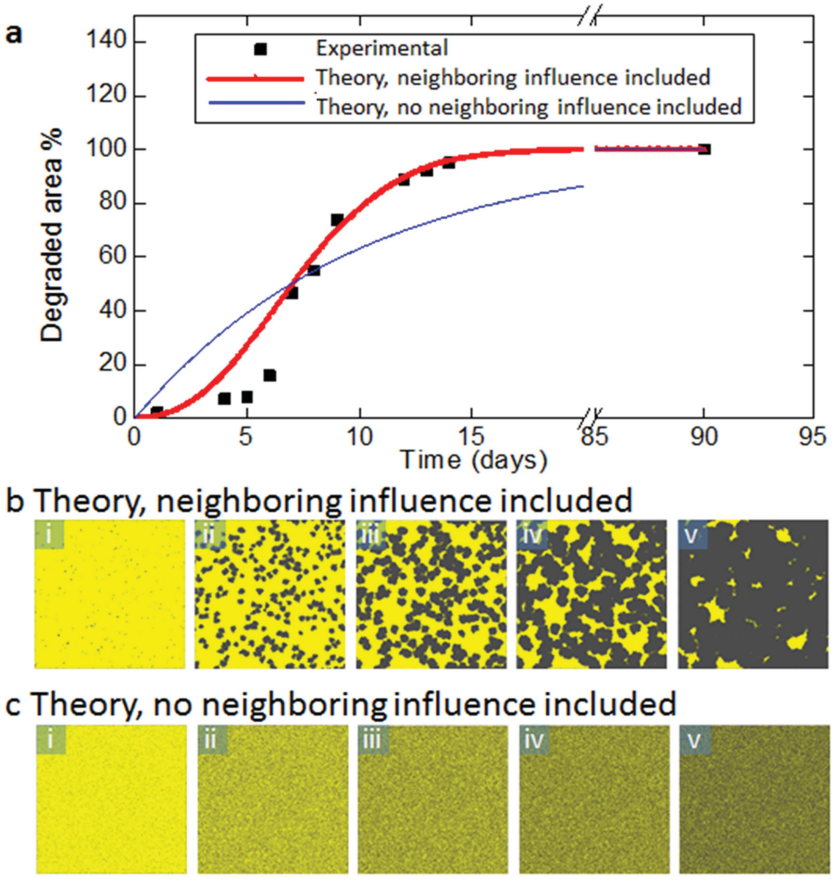


**Figure 3.** Experimental (black squares) and simulated degraded area percentages including neighboring interaction (solid red lines) and with neighboring interactions disregarded (blue red lines). Stages of simulated sample surface during the degradation process b) correspond to red curve and c) correspond to blue curve.

To further understand the degradation process, we use a variant of the forest-fire model to fit our experimental data. We divide the sample surface in $N \times N$ square elements, each of which may exist in one of the two states: undegraded BP or degraded BP. Let $\eta^{(n)}$ be the degradation probability per unit time of a surface element that has $n$ degraded neighbors $(0 \le n \le 8)$. Consequently, the degradation probability after a small but finite time interval $\Delta t$ is equal to $P_n = 1 - e^{-\Delta t \cdot \eta^{(n)}}$. For simplicity, we assume that each degraded neighbor increases $\eta^{(n)}$ by a fixed amount $\Delta\eta$, that is, $\eta^{(n)} = \eta^{(0)} + n\Delta\eta$, where $\eta^{(0)}$ is the degradation probability per unit time if all the immediate neighbors are in the undegraded BP state. We note that our model operates with the degradation probabilities, $\eta^{(n)}$, which can be related to chemical processes that accompany the degradation process such as chemical reaction of BP with $O_2$ and $H_2O$ to form oxidized phosphorus species. In this way, the model can be used to predict the degradation time evolution under different environmental conditions with varying content of $O_2$ and $H_2O$. In the current work, however, we used $\eta^{(n)}$ merely as a fitting parameter. We found a good fit to the experimental results, shown in Figure 3, using $\eta^{(0)} = 0$ and $\Delta\eta = 0.45\text{d}^1$. For convergence, it was sufficient to use $N = 512$ and $\Delta t = 90$ min. We note that if we neglect the influence of neighbors on the degradation probabilities by setting $\Delta\eta = 0$, the model does not predict the experimentally observed

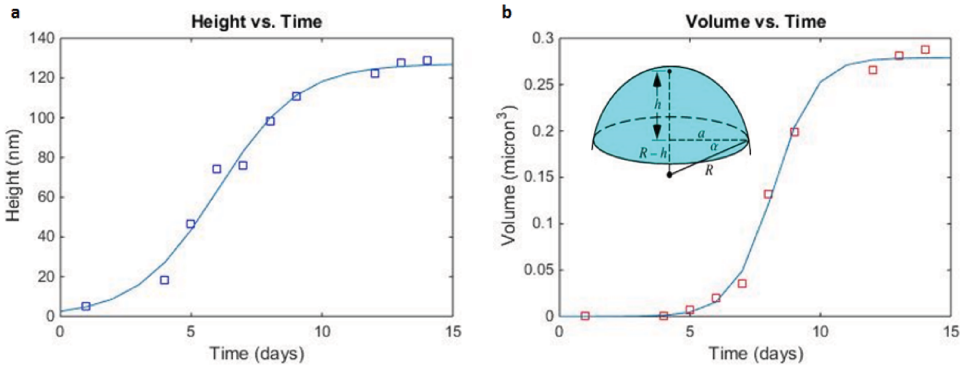


**Figure 4.** Experimental (squares) and simulated (solid lines) of results of a) height and b) volume of a degraded bubble. Volume is calculated according to the geometry shown in the inset of (b).

results as shown by the blue curve in Figure 3, which is qualitatively different from the measured fraction of degraded surface. Our model strongly suggests that the influence of degraded surface elements on non-degraded ones critically contributes to the degradation process of BP. We also show that $\Delta\eta \neq 0$ leads to the formation of degraded clusters (Figure 3b), while neglecting the influence of degraded neighbors results in a homogeneous distribution of degraded surface elements (Figure 3c). Thus, taking the influence of degraded neighbors into account qualitatively reproduces experimental images (Figure 2).

When BP chemically degrades, in addition to the increase of the degraded area, the height of the degraded bubbles also increases vertically on the sample surface. By selecting a single degraded bubble, we have measured the height and volume of the degraded regions as a function of time as shown in **Figure 4**. To get each experimental data point (open rectangles) in Figure 4, the height of the degraded particles was measured from a topographic line profile, and the volume of a bubble was approximated by a spherical cap of height $h$ and base radius $a$, as shown in the inset of Figure 4b. Base radius was measured by drawing three different lines across the center and the average value is used in the formula $V = \frac{\pi h}{6}\left(3a^2 + h^2\right)$ of the spherical cap. We found that both the height (Figure 4a) and the volume (Figure 4b) of the degraded regions increase slowly initially and grow in an exponential fashion before reaching saturation growth. Since the modified forest-fire model introduced above is only appropriate for a surface area analysis, we cannot apply it to the experimental height and volume data shown in Figure 4. However, we used the well-known sigmoid (S-shaped) growth curve to fit the experimental results, as shown by the solid lines in the Figure 4a,b.

There is excellent agreement between the experimental and the S-shaped growth curves. Although the S-shaped growth curve, in our case, does not provide any direct physical insight, such as, the contribution of neighborhood interactions introduced above using the modified forest-fire model, the curve fit provides the growth saturation value, the steepness of the growth, and the mid-point of the growth, via the three fit parameters typical to S-curves: $k$, $r$, and $t_0$, respectively. The obtained fitting curves for height and volume are shown in Figure 4a,b. From the height fit (the solid line in Figure 4a), we obtained a saturation height of $k$ = 127.21 nm, a maximum growth steepness of $r = \ddot{0}.65\ \mathrm{d}^{-1}$, and a mid-point of the growth of $t_0$ = 6.01 d, which is the time it takes to grow the height to 50% of its saturation value. For the volume curve, we obtained a saturation volume of 0.28 μm$^3$, and the steepness of the volume growth was 1.27 d$^{-1}$, reaching the 50% of its saturation value within 8.21 d. Although the exact mechanism of the (height/volume) enlargement is beyond the scope of this paper, these fit parameters and the S-curve fit in general may shed light on the 3D growth evolution.

It has been shown that coating BP with $Al_2O_3$ can passivate from ambient degradation.[8] However, the dependence of the coating effectiveness on its thickness was not studied. Here, we investigate several BP flakes coated with 1, 5, 10, 20, and 50 nm thick $Al_2O_3$ in order to study the effectiveness of the coating in protecting ambient degradation as a function of size over a long period of time. **Figure 5** shows the evolution of topography and optical near-field images of the two 5 nm thick flakes coated with 1 nm thick $Al_2O_3$ layer over a span of 65 d. We found that despite the 1 nm protective layer, the underlying BP flake degrades in both cases but at a much reduced rate compared to uncoated samples presented in Figure 2. In Figure 5a–h, the degradation starts at the edges of the flake, as well as holes that randomly begin on the surface of the coated layer as clearly seen on the 3D topographic images shown in Figure 5q–r. In Figure 5e–h,m–p, we show another 10 nm high BP flake that also coated with 1 nm thick $Al_2O_3$. In this flake degradation starts from the edges of the flake and grows inward. We have observed similar degradation of several 1 nm $Al_2O_3$ coated BP flakes with varying thicknesses.

We have also studied the effectiveness of a 5 nm thick $Al_2O_3$ coating (**Figure 6**) on a 10 nm thick BP flake. We found, similar to our observations in Figure 5, that the BP sample continues to degrade at a yet slower rate than that in the case of a 1 nm coating. The BP flake studied in Figure 6, initially had randomly scattered nanometer-size degraded bubbles (which possibly arose during/between exfoliation and coating). These initial degraded regions continue to grow at a slow rate and increase in size, as shown in Figure 6e,j. In Figure 6k, the rectangular points present the measured evolution of the degraded area fraction, while the solid line is the theoretical fit. The degraded area was measured following the same procedure as we used to obtain the area shown in Figure 3. In comparison to Figure 2 (uncoated sample) and Figure 5 (1 nm $Al_2O_3$ coated sample), it

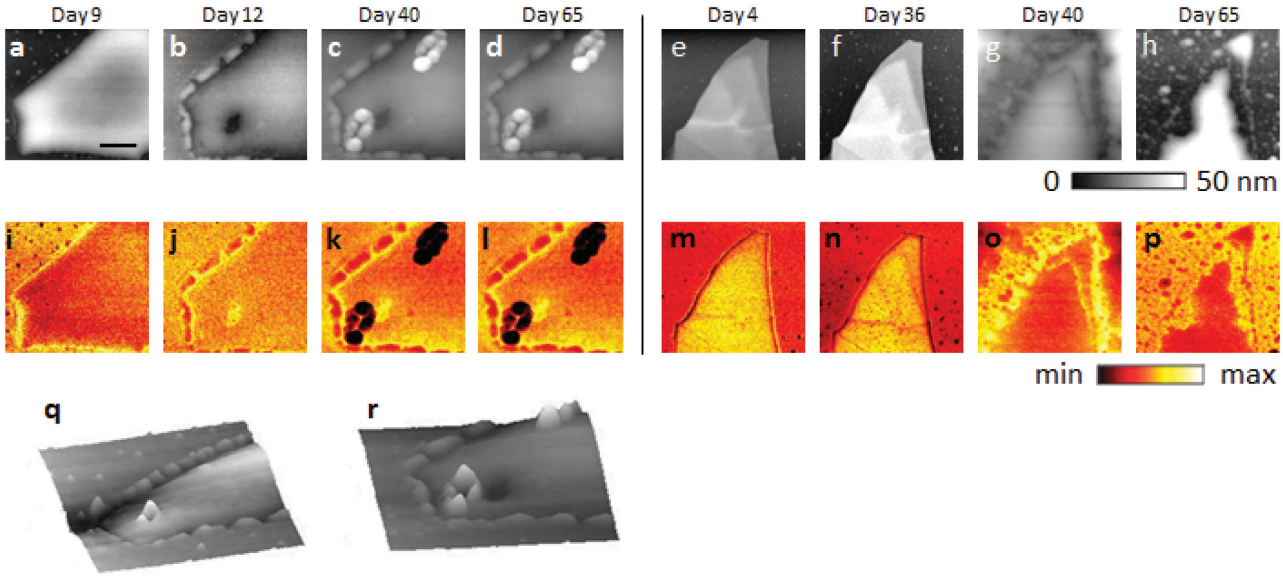


**Figure 5.** a–h) Topography and i–p) third harmonic near-field amplitude images of two different flakes of thickness ≈5 nm, coated with a 1 nm coating layer of $Al_2O_3$; q,r) 3D topographic images of (b) and (c), respectively.

can be clearly seen that the degradation takes place at a slower rate due to the larger thickness (5 nm) of the $Al_2O_3$ coating. However, since the degradation still increases with time, it is evident that even 5 nm coating of sapphire is insufficient to be considered an ideal passivation of BP underneath it.

We further investigated the effectiveness of thicker $Al_2O_3$ coatings (thickness 10 nm or more) on various thickness BP flakes by following the degradation behavior over a long period of time. **Figure 7**a–j shows the topography and near-field optical images of the evolution of 10 nm $Al_2O_3$ coated 5 nm thick BP flakes. We have also studied 20 and 50 nm thick $Al_2O_3$ coating as shown in Figure 7k–p. We found no trace of degradation over a long period of time (>3 months) in all of these samples, which indicates that thicker (10 nm or larger) coating is necessary when using coating of BP by $Al_2O_3$ using ALD for enhanced passivation of BP over an extended period of time.

In summary, we have extensively investigated ambient degradation of exfoliated BP with and without a thin $Al_2O_3$ coating layer using the unique simultaneous topographic and nanoscale spectroscopic imaging capabilities of s-SNOM. By measuring several BP flakes coated with varying thickness $Al_2O_3$ deposited by ALD over a span of several months, we show that the degraded area and volume increase with time slowly in the beginning of degradation and grow rapidly (approximately exponentially) afterward before reaching saturation growth following S-shaped growth curve (sigmoid growth curve). Our theoretical modeling of the experimental degradation growth pattern shows that the influence of degraded areas on their adjacent environment is the cause of the observed exponential growth at the initial stage of degradation growth pattern. We found that the thickness and quality of coating are critical to effectively passivate BP from ambient degradation. Oxidized phosphorus species, chemically identified using nanoscale

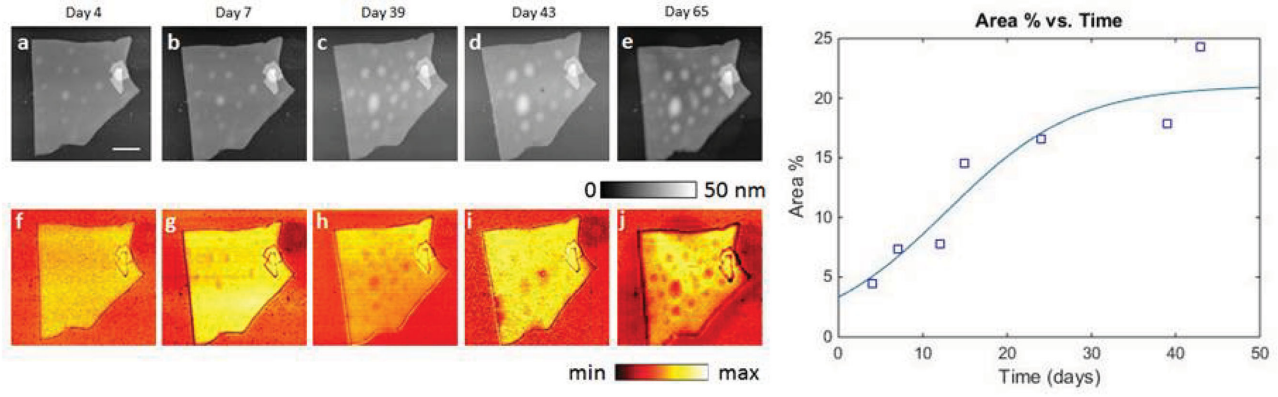


**Figure 6.** a–e) Topography and f–j) third harmonic near-field amplitude images of 10 nm BP flake coated with ≈5 nm thick $Al_2O_3$. Experimental (open squares) and simulated (solid blue line) results of area fraction of the degraded surface.

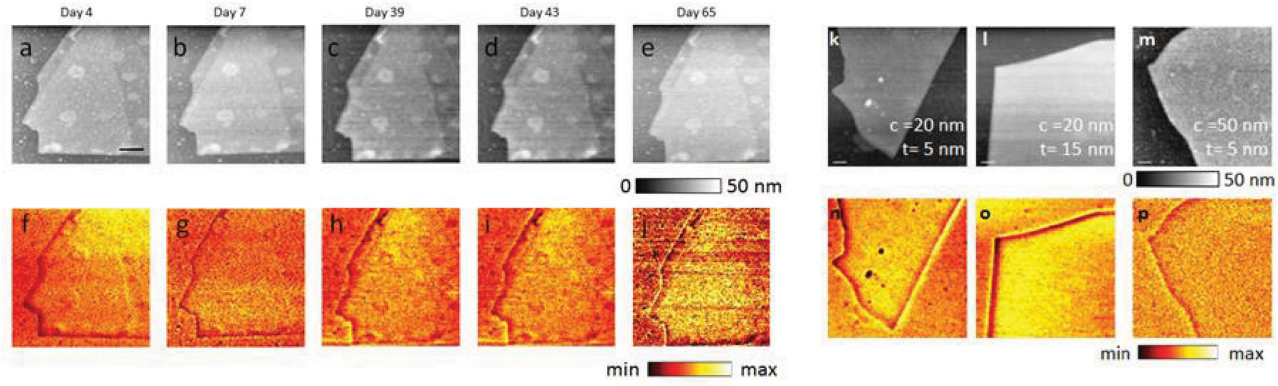


**Figure 7.** a–e) Topography and f–j) $A_2$ images of a 5 nm thick BP flake coated with a sapphire layer of 10 nm. k–m) Topography and n–p) near-field amplitude images on day 65 of three flakes of different thicknesses, *t* and different sapphire coating layer, *c*; the values of *t* and *c* are given in each image from (k) to (m).

spectroscopic imaging by s-SNOM, can still form underneath 5 nm or less thick $Al_2O_3$ coating, which renders thin coatings insufficient to protect BP against degradation.

## Acknowledgements

The work was supported by a grant from the Air Force Office of Scientific Research. S.G. acknowledges support by NSF Award No. 1553251. Z.L. acknowledges the support of DOE Award No. DEFG02-07ER46376 and S.B.C acknowledges support by NSF Award No. 1402906.

Received: February 10, 2016
Published online: May 17, 2016

[1] L. Li, Y. Yu, G. J. Ye, Q. Ge, X. Ou, H. Wu, D. Feng, X. H. Chen, Y. Zhang, *Nat. Nanotechnol.* **2014**, *9*, 372.
[2] F. Xia, H. Wang, Y. Jia, *Nat. Commun.* **2014**, *5*, 4458.
[3] X. Ling, H. Wang, S. X. Huang, F. N. Xia, M. S. Dresselhaus, *Proc. Natl. Acad. Sci. USA* **2015**, *112*, 4523.
[4] J. Kim, S. S. Baik, S. H. Ryu, Y. Sohn, S. Park, B.-G. Park, J. Denlinger, Y. Yi, H. J. Choi, K. S. Kim, *Science* **2015**, *349*, 723.
[5] Y. Abate, S. Gamage, L. Zhen, S. B. Cronin, H. Wang, V. Babicheva, M. H. Javani, M. I. Stockman, *arXiv:1506.05431* [cond-mat.mes-hall].
[6] R. Fei, L. Yang, *Nano Lett.* **2014**, *14*, 2884.
[7] X. Wang, A. M. Jones, K. L. Seyler, T. Vy, Y. Jia, H. Zhao, H. Wang, L. Yang, X. Xu, F. Xia, *Nat. Nanotechnol.* **2015**, *10*, 517.
[8] J. D. Wood, S. A. Wells, D. Jariwala, K. S. Chen, E. Cho, V. K. Sangwan, X. L. Liu, L. J. Lauhon, T. J. Marks, M. C. Hersam, *Nano Lett.* **2014**, *14*, 6964.
[9] J. Dai, X. C. Zeng, *RSC Adv.* **2014**, *4*, 48017.
[10] J. M. Stiegler, Y. Abate, A. Cvitkovic, Y. E. Romanyuk, A. J. Huber, S. R. Leone, R. Hillenbrand, *ACS Nano* **2011**, *5*, 6494.
[11] R. Hillenbrand, F. Keilmann, *Appl. Phys. Lett.* **2002**, *80*, 25.
[12] I. J. M. H. Zwietering, F. M. Rombouts, K. van't Riet, *Appl. Environ. Microbiol.* **1990**, *56*, 1875.
[13] A. Cvitkovic, N. Ocelic, J. Aizpurua, R. Guckenberger, R. Hillenbrand, *Phys. Rev. Lett.* **2006**, *97*, 060801.